Journal of Materials Chemistry A

Accepted Manuscript

ROYAL SOCIETY OF CHEMISTRY

www.rsc.org/materialsA

Journal Name

ARTICLE

Manipulation of Optical Field Distribution in ITO-free Micro-cavity Polymer Tandem Solar Cell *via* the Out-of-cell Capping layer for High Photovoltaic Performance

Received 00th January 20xx,
Accepted 00th January 20xx

DOI: 10.1039/x0xx00000x

www.rsc.org/

Lijian Zuo,[ab]† Chih-Yu Chang,[a]† Chu-Chen Chueh,[a] Yunxiang Xu,[a] Hongzheng Chen*[b] and Alex K.-Y. Jen*[ab]

Series-connected tandem organic photovoltaics (SCTOPVs) have been shown to provide higher power conversion efficiencies (PCEs) than the single junction devices due to the improved light harvesting. To achieve the optimal device performance of SCTOPV, balancing the photocurrents generated from the sub-cells is critical according to the Kirchhoff law. In this work, we demonstrate that the out-of-cell capping layer of an ITO-free microcavity SCTOPV plays an important role on manipulating the optical field distribution in the constituent sub-cells for achieving balanced photocurrents and the optimal photovoltaic performance. Two mirror-like electrodes, a semi-transparent ultrathin Ag capped with a dielectric TeO_2 layer and a thick Ag electrode were used to construct an ITO-free top-illuminated microcavity configuration, in which certain frequencies of solar irradiance can resonate between the reflective surfaces. As a result, a top-illuminated ITO-free SCTOPV with a comparable performance (7.4%) to ITO-based counterpart (7.5%) was demonstrated despite the inferior transmittance of the ultra-thin Ag relative to ITO.

1. Introduction

Photovoltaics that can efficiently convert solar irradiation into electrical power have been investigated worldwide as a possible solution for sustainable energy source.[1] Among all solar energy conversion techniques that have been exploited so far, organic photovoltaics (OPVs) is one of the important focus due to their good mechanical flexibility, light-weight, and low-cost.[2,3] However, for the practical applications, further improvements in their device performance and reduction in production cost are critical.

Thus far, most state-of-the-art OPVs are fabricated with bulk heterojunction (BHJ) structures,[4,5] which typically consists of an electron donor polymer blended with an electron acceptor. Limited by the low carrier mobility and high exciton binding energy of organic materials, the optimized BHJ layer thickness is usually restricted to ~100 nm, which is not sufficient to fully absorb the solar irradiation.[4] This coupled with its narrowband absorption feature thereby results in a significant transmittance loss.[6] One possible approach to improve light-harvesting efficiency is to develop mutli-junction tandem configurations, which are typically series-connected to prolong the light traveling pathways and to take advantage of complementary absorption from the constituent sub-cells.[3,6,7] For the series-connected tandem OPVs (SCTOPVs), it is essential to obtain balanced short circuit current density (J_{SC}) between the sub-cells for achieving the maximum power output (namely, maximum efficiency) according to the Kirchhoff law, provided that the J_{SC} of a tandem device is governed by the smallest value of the constituent sub-cell.[8] In this regard, employing complementary absorbing materials in different sub-cells[9] or optical manipulation techniques,[10] such as plasmonics effect[11] and micro-cavity effect[12], have been extensively utilized to achieve the balanced J_{SC}s between the sub-cells for maximizing the photovoltaic performance of SCTOPVs.

Most recently, using optical micro-cavity in single junction OPVs has been appeared an effective approach to modulate the light confinement and optical field distribution in the devices.[13-15] The micro-cavity configuration is generally composed of two mirror-like electrodes, such as Ag, where the resonant light would oscillate in between until fully absorbed by the photoactive materials. Although the reflective ultra-thin Ag would cause reflection loss at the light in-coming side, the conjunction with a high refractive index capping layer, like tellurium oxide (TeO_2, n ~2.2), can effectively suppress it and increase the light in-coupling into the device.[13,16] In principle, the compromise between the reflection loss and micro-cavity enhancement determines the efficacy of this resonant cavity. It is worthy to note that the micro-cavity based devices can feature adjustable optical field distribution within its micro-

[a] Department of Materials Science and Engineering, University of Washington, Seattle, USA. E-mail: ajen@u.washington.edu.
[b] State Key Laboratory of Silicon Materials, MOE Key Laboratory of Macromolecular Synthesis and Functionalization, Department of Polymer Science & Engineering. Email ajen@u.washington.edu, hzchen@zju.edu.cn:
† These authors contributed equally.
Electronic Supplementary Information (ESI) available: Single junction device fabrication procedure, thickness dependent device performance, optical simulation. See DOI: 10.1039/x0xx00000x

cavity chamber through the careful control of each constituent interlayers' thickness, including the capping layer, ultra-thin Ag layer, and photoactive layer.[13,15-17] Therefore, the integration of the micro-cavity chamber into a tandem device can simultaneously enhance light-trapping and manipulate optical field distribution in each sub-cell for better photo-current matching. More importantly, this micro-cavity configuration can afford the ITO-free advantage, making itself more cost-effective and compatible with large-area, roll-to-roll processing. Nonetheless, this device structure is still not so commonly employed so far.[18]

In this work, we demonstrate a highly efficient polymer tandem solar cell based on an ITO free, micro-cavity structure (Figure 1). Ultra-thin Ag capped with a 30 nm TeO_2 thin layer was used as the transparent electrode in this structure. The device structures of ITO- and ultra-thin Ag-based tandem solar cells are shown in Figure 1a-b, respectively. BHJ layers with complementary absorption spectra were chosen in the studied tandem architectures, where poly(indacenodithieno[3,2-b]thiophene-alt-difluoro-quinoxaline) (PIDTT-DFQT): [6,6]-phenyl-C71-butyric acid methyl ester ($PC_{71}BM$) served as the BHJ of the front sub-cell while the poly(cyclopentadithiophene-alt-fluoro-benzothiadiazole) (PCPDT-FBT):$PC_{71}BM$[19,20] was used as the BHJ of the back sub-cell (Figure 1c).

Two sub-cells were electrically series-connected via the interconnection layer (ICL) consisting of poly(3,4-ethylene-dioxythiophene):poly(styrenesulfonate) (PEDOT:PSS)/ZnO composite film. It is unveiled that the optical field distribution within each sub-cell of the ITO-based SCTOPV is not ideal, although the high transmittance of ITO allows large portion of solar irradiation to enter the device. The solar irradiation intensively localized in the back sub-cell and resulted in severe optical loss, leading to mismatched JSC between each sub-cells. However, for the micro-cavity based SCTOPV, the J_{SC} of each sub-cell is more balanced and enhanced light-trapping in BHJ layers can be accomplished by fine-tuning the thickness of the employed capping layer. As a result, the J_{SC} of the micro-cavity based device is comparable to that of the ITO-based device regardless of the inferior transmittance of ultra-thin Ag relative to ITO. Finally, an ITO-free SCTOPV with a high PCE of ~7.4% was successfully demonstrated which is comparable to that of ITO-based counterpart. Considering the low-cost and better mechanical properties of ultra-thin Ag, this work provides new device architecture for making highly efficient printable SCTOPV.

2. Experimental Section

2.1 Optical simulation

In order to evaluate and investigate the individual contribution of each layer within the device upon optical absorption, optical simulations based on the transfer matrix formalism (TMF) are used to calculate the interference of reflected and transmitted light at each interface within the stratified devices. The wavelength-dependent optical properties of each layer is represented by the index of refraction (ñ = n + ik) of each material, acquired by variable angle spectroscopic ellipsometry (VASE). All the simulations are based on the assumptions of planar interfaces and total isotropy for all layers. However, the interference within the glass substrates is ignored because their thicknesses (2 mm) are much higher than the wavelengths of the simulated incident beams. The C60-self assembly monolayer (C_{60}-SAM) is also ignored due to the ultra-thin thickness. For each device structure, the optical simulation adopt exactly the same layer thickness as those used in practical device fabrication. In addition, 100% internal quantum efficiency (IQE) and the AM1.5 intensity spectrum (ASTM G173-03) are assumed to calculate the theoretically maximum photocurrent density. In order to compensate the deviation resulted from the 100% IQE assumption, mismatch factors of 0.95 and 0.61 are applied to the PIDTT-DFQT and PCPDT-FBT based single junction solar cells. The mismatch factor for PIDTT-DFQT based solar cell was obtained according to the fact that the measured J_{SC} is 11.4 mA/cm^2 and the calculated J_{SC} is 12.1 mA/cm^2 in single junction devices. At the same time, the measured J_{SC} of single junction PCPDT-FBT based device is 14.2 mA/cm^2 while

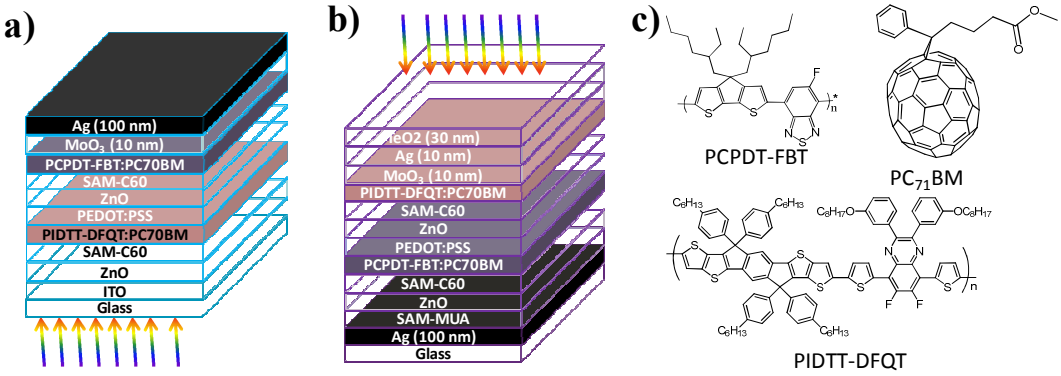

Figure 1. Schematic device configurations of a) ITO-based tandem solar cell and b) Ultra-thin Ag based top-illuminated tandem solar cell. c) Molecular structures of PCPDT-FBT, PIDTT-DFQT, and $PC_{71}BM$.

calculated to be 23.6 mA/cm^2.

2.2 Fabrication of ITO based tandem devices

ITO glass substrates were cleaned by de-ionic water, acetone, iso-propanol in ultra-sonic bath. After treated by plasma for 15 min, ZnO precursor solution was spin-coated in glove box and annealing in air at 130 ^{o}C for 5 min. Subsequently, C_{60}-SAM was spin-coated on ZnO. PIDTT-DFQT:$PC_{71}BM$ solution (1:4 wt%, o-dichlorobenzene (DCB), 3% 1-chloronaphthalene (CN)) was spin-coated at 800 rpm to form ~100 nm film (calibrated by atomic force microscopy (AFM)). After annealed at 110 ^{o}C for 5 min, the films were spin-coated with modified PEDOT:PSS in ambient air and annealed at 150 ^{o}C for 5 min. After that, highly conductive PEDOT:PSS (PH 1000) was spin-coated at 5 krpm and annealed in glove-box at 150 ^{o}C for 5 min. The low modified PEDOT:PSS(4083) is used to extract the hole and block electron from the bottom cell. The high conductive PEDOT:PSS (PH1000) is used to form respectable electric contact to enable efficient electron/hole recombination from the sub-cells. Since these two PEDOT:PSS layers are deposited sequentially, possible intermixing between them is expected to occur. In this regard, we consider these two PEDOT:PSS layers as a whole. Following that, ZnO was spin-coated and annealed at 130 oC for 5 min in glove-box to form a 20 nm film and assembled with mono-layer C_{60}-SAM. PCPDT-FBT:$PC_{71}BM$ solution (1:2.5 wt%, 1,2,4-trichlorobenzene, 21 mg/ml) were spin-coated at 900 rpm for 5 min and annealed at 100 ^{o}C for 5 min. Finally, the substrates were transferred into vacuum chamber to deposit 10 nm MoO_3 and 100 nm Ag.

2.3 Fabrication of ITO-free micro-cavity devices

Glass substrates were cleaned with the same procedure as ITO glass. After treated in air plasma for 15 min, patterned Ag were deposited. After assembled with mono-layer 11-Mercaptoundecanoic acid (MUA), 20 nm ZnO and C_{60}-SAM layers were deposited as previous procedures. On top of these substrates, 80 nm PCPDT-FBT:$PC_{71}BM$, ICL (m-PEDOT:PSS/PEDOT:PSS-PH1000/ZnO/C_{60}-SAM) and 100 nm PIDTT-DFQT:$PC_{71}BM$ film were deposited sequentially following the previous procedures. Finally, 10 nm ultra-thin Ag were deposited to complete Device B and additional 30 nm TeO_2 were deposited to complete Device E.

2.4 Device characterization

The J–V characteristics were recorded using a Keithley 2400 source meter. A 300 W xenon arc solar simulator with an AM 1.5 global filter operated at 100 mW cm^{-2} was used to simulate the AM 1.5G solar irradiation for the J-V measurements. The illumination intensity was corrected by using a silicon photodiode with a KG5 color filter calibrated by the National Renewable Energy Laboratory (NREL).

2.5 Materials

All the materials are from Sigma-Aldrich Corp., and used as received without specification. The PCBM is from American Dye Corp. and the donor materials and C_{60}-SAM in this work are home-made.

3. Results and Discussion

3.1 Single junction device

To efficiently utilize solar irradiation, two conjugated polymers with complementary absorption spectra, PIDTT-DFQT[21] and PCPDT-FBT,[19] were used as the polymer donors in BHJ layers in this study. Figure 2 showed the UV-visible absorption spectra of PIDTT-DFQT:$PC_{71}BM$ and PCPDT-FBT:$PC_{71}M$ films. The PIDTT-DFQT based BHJ has an absorption band edge of ~700 nm while the PCPDT-FBT based BHJ can absorb light to ~870 nm. In the tandem device structure, the higher energy photons were primarily absorbed by the PIDTT-DFQT:$PC_{71}BM$ front cell to generate large V_{OC}, while the transmitted lower energy photons were further absorbed by the low band-gap PCPDT-FBT:$PC_{71}M$ back sub-cell. In such sequence, the thermalization loss of “hot excitons” generated by higher energy photons can be effectively reduced, which is beneficial to achieve maximum open circuit voltage (VOC) and performance of STCOPV.

The evaluation and optimization of the single junction devices, e.g. BHJ thicknesses and interfacial layers, are critical to the photovoltaic performance of the derived SCTOPV. Therefore, single junction solar cells (device structure: ITO/ZnO/C_{60}-SAM/BHJ/MoO_3/Ag, defined as Device A) were fabricated. Note that a C_{60}-SAM layer was used to passivate ZnO surface traps and enhance the electronic coupling between ZnO and BHJ layer.[22] The current–voltage (J-V)

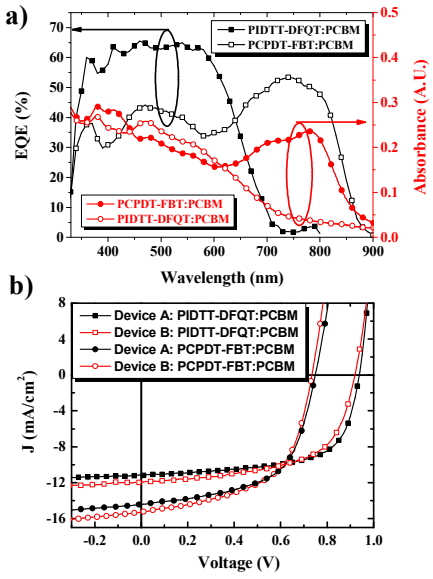

Figure 2. a) Absorption and EQE spectra of PIDTT-DFQT:PC71BM and PCPDT-FBT:PC71BM BHJ film and single junction devices (Device A), and b) J-V characteristics of inverted (Device A) and top-illuminated single junction solar cells (Device B) of PIDTT-DFQT:PC71BM and PCPDT-FBT:PC71BM.

characteristics of the devices measured under AM1.5 illumination were in Figure 2b and S1, and the corresponding device parameters were summarized in Table 1. It was clearly shown the optimized PCE is achieved at a particular BHJ thickness due to the compromise between J_{SC} and fill factors (FF) for both PIDTT-DFQT:$PC_{71}BM$ and PCPDT-FBT:$PC_{71}BM$ devices. This is consistent with the prior statement that a thicker BHJ layer tends to encounter severe bimolecular charge recombination due to the space charge effect and that a thinner layer causes severe optical loss and leakage current.[23]

At the optimized BHJ thickness, the PIDTT-DFQT:$PC_{71}BM$ single junction device exhibited a V_{OC} of 0.91 V, a J_{SC} of 11.17 mA/cm^2, a FF of 0.64, and a PCE of 6.54% while the PCPDT-FBT:$PC_{71}BM$ device showed a V_{OC} of 0.74 V, a J_{SC} of 14.12 mA/cm^2, a FF of 0.60, and a PCE of 6.17%. The high V_{OC} (0.91 V) shown in PIDTT-DFQT:$PC_{71}BM$ device indicates its capability to reduce the thermalization loss and serve as an efficient front sub-cell in a SCTOPV. The EQE spectra of PIDTT-DFQT:$PC_{71}BM$ device between 300 and 700 nm shows a maximum value of 68%, contributing to an integrated J_{SC} of 10.6 mA/cm^2 while the EQE spectra of PCPDT-FBT:$PC_{71}BM$ device between 300 and 870 nm exhibits a maximum value of 55%, leading to an integrated J_{SC} of 13.3 mA/cm^2. The complementary EQE spectra shown by these two devices, consistent with their absorption spectra (Figure 2a), is important to achieve balanced J_{SC} in sub-cells for SCTOPV.

Table 1. Device parameters of single junction device of PIDTT-DFQT:PC71BM and PCPDT-FBT:PC71BM.

Active layer	d[c] [nm]	J_{SC} [mA/cm^2]	V_{OC} [V]	FF [/]	PCE[d] [%]
PCPDT-FBT:$PC_{71}BM$ [a]	122	12.21	0.73	0.54	4.81(4.42±0.26)
	97	14.29	0.74	0.54	5.72(5.21±0.31)
	75	14.12	0.74	0.60	6.17(5.79±0.25)
	64	13.18	0.74	0.58	5.62(5.42±0.11)
	46	11.46	0.68	0.44	3.43(3.16±0.21)
Micro-cavity[b]	80	15.07	0.73	0.56	6.21(5.91±0.21)
PIDTT-DFQT:$PC_{71}BM$ [a]	124	11.27	0.88	0.53	5.22(4.92±0.17)
	96	11.39	0.90	0.63	6.46(6.22±0.16)
	81	11.17	0.92	0.64	6.54(6.32±0.11)
	67	10.22	0.92	0.65	6.03(5.52±0.29)
Micro-cavity[b]	70	11.92	0.91	0.60	6.56(6.02±0.41)

[a]Device A: ITO/ZnO/C_{60}-SAM/Active layer/MoO_3/Ag; [b]Device B: glass/Ag(100 nm)/MUA-SAM/ZnO/C_{60}-SAM/Active layer/MoO_3/Ag; [c]active layer thickness; [d]the PCE values outside of parentheses are the best device performance, and those inside indicate the averaged value and standard deviation.

3.2 Single junction micro-cavity devices

Adopting micro-cavity configuration in the device has been demonstrated as an effective light confinement strategy for improving photo to electron response in single junction OPVs. To gain more insight for the micro-cavity based architecture, we have further fabricated single junction micro-cavity devices based on the configuration of glass/Ag/ZnO/C_{60}-SAM/BHJ/MoO_3/ultra-thin Ag/TeO_2, referred as Device B. The optical micro-cavity chambers were formed due to high reflectivity of the transparent ultra-thin Ag and the opaque Ag back electrode. Optical simulation was conducted to realize the optical field distribution and J_{SC} of the devices[24] (See the experimental section for the detailed information of optical simulation). It was assumed that the absorbed photons are fully converted into electrons in simulation, namely 100% internal quantum efficiency (IQE). Figure 3 showed the dependence between J_{SC} of Device B and various thicknesses of the capping layer, BHJ layer, and ultra-thin Ag layer, (a-c,

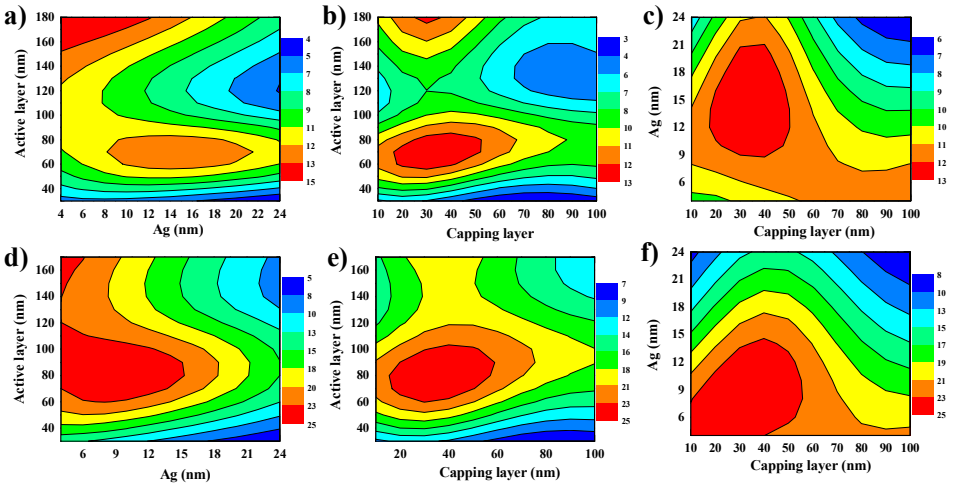

Figure 3. Variation of J_{SC} of PIDTT-DFQT:$PC_{71}BM$ single junction device with: a) thickness of BHJ layer and transparent Ag layer, while fixed the capping layer at 30 nm, b) thickness of capping layer and BHJ layer, while fixed the ultra-thin Ag at 14 nm, c) thickness of Ag layer and the capping layer, while fixed the BHJ layer at 70 nm. Variation of J_{SC} of PCPDT-FBT:$PC_{71}BM$ single junction device with: d) thickness of BHJ layer and transparent Ag layer, while fixed the capping layer at 40 nm, e) thickness of capping layer and BHJ layer, while fixed the ultra-thin Ag at 10 nm, f) thickness of Ag layer and the capping layer, while fixed the BHJ layer at 80 nm.

PIDTT-DFQT:$PC_{71}BM$ based device; d-f, PCPDT-FBT:$PC_{71}BM$ based device). As shown, the maximum J_{SC} of PIDTT-DFQT:$PC_{71}BM$ devices could be achieved using a 70 nm thick BHJ layer with a 30 nm thick capping TeO_2 and a 14 nm thick Ag, respectively. For the PCPDT-FBT:$PC_{71}BM$ system, the thickness of BHJ layer, TeO_2, and Ag for achieving optimal J_{SC} is 80 nm, 40 nm, and 10 nm, respectively.

Here, we take the PIDTT-DFQT:$PC_{71}BM$ based device as a model to study the properties of the optical micro-cavity structure. Different to the ITO based transparent electrode, the ultra-thin Ag film is highly reflective. When the ultra-thin Ag layer was used as the transparent electrode, the high reflectivity of Ag would induce severe surface reflection loss. On the other hand, the introduction of an optical micro-cavity will significantly improve light-trapping. Increasing the thickness of this Ag layer will strengthen both effects. Figure S2 showed the dependence of Ag layer thickness on light intensity distribution and the simulated EQE spectra of PIDTT-DFQT:$PC_{71}BM$ based micro-cavity (Device B). With a 8 nm thick Ag, the simulated EQE resembles to the absorption spectra of PIDTT-DFQT:$PC_{71}BM$ film.

The effect of micro-cavity becomes stronger when the Ag thickness increases. As a result, the light absorption between 550-700 nm becomes stronger. However, the reflection loss from the non-resonant light also becomes significant when the thickness of Ag layer is increased. Severe optical reflection loss is induced in wavelengths between 350-500 nm. As a result of balance between reflection loss and enhanced light-trapping, the highest J_{SC} could be achieved at an optimal Ag thickness of 14 nm for PIDTT-DFQT:$PC_{71}BM$ device and 10 nm for the PCPDT-FBT:$PC_{71}BM$ device, respectively. The variations of optimal Ag thickness for PIDTT-DFQT:$PC_{71}BM$ and PCPDT-FBT:$PC_{71}BM$ devices stem from their different absorption profiles. In general, the combined thickness of BHJ and interfacial layers determines the oscillating wavelengths in the micro-cavity chamber. Figure S3 showed the relationship between the light intensity distribution and BHJ thickness, and the simulated EQE spectra of PIDTT-DFQT:$PC_{71}BM$ micro-cavity devices (Device B). If the BHJ thickness is increased, the resonant light wavelengths will be red-shifted. For BHJ layers with distinct absorption profiles, different oscillating wavelengths are required in order to maximize the effect of light-trapping in the micro-cavity chamber, which determines the corresponding optimized BHJ thickness. This explains the observation of differently optimal BHJ thickness in PIDTT-DFQT:PC71BM (70 nm) and PCPDT-FBT:$PC_{71}BM$ (80 nm).

Based on the Equation S1-S5 in SI, a capping TeO_2 layer was deposited on top of Ag to reduce the reflection loss at the light incoming side. The light intensity distribution of micro-cavity based device with various TeO_2 thicknesses is illustrated in Figure S4. As shown, without TeO_2, the reflectivity of Ag is strong and the light intensity distribution is concentrated in the region between 550 and 700 nm, which corresponds well with the absorption peak at 630 nm in the simulated EQE. However, the device suffered a significant reflection loss in the region between 330 and 550 nm. After depositing an ultra-thin TeO_2 layer (10 nm), the surface reflection loss was largely reduced, without significantly influencing the micro-cavity region (630 nm). When the TeO_2 thickness was further increased, the micro-cavity induced resonance became weaker in spite of the further reduction in reflection loss. After compromising these tow parameters, an optimal light utilization could be achieved if a 30-40 nm thick TeO_2 capping layer was implemented for both PIDTT-DFQT:$PC_{71}BM$ and PCPDT-FBT:$PC_{71}BM$ based devices to obtain the highest J_{SC} (Figure S4).

Based on the optical simulations, we further fabricated the corresponding micro-cavity devices. The J-V characteristics of

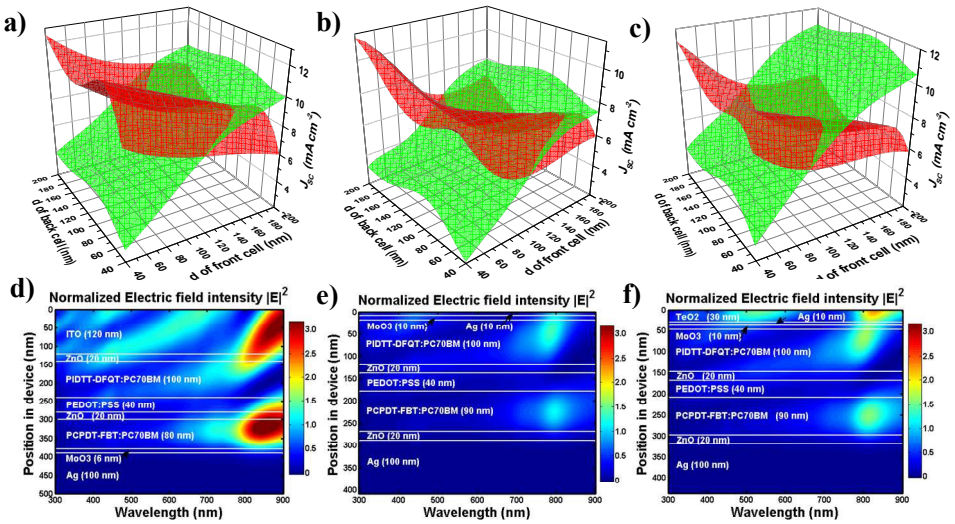

Figure 4. The sub-cells active layer thicknesses dependent JSC of front and back sub-cell (green surface for the front cell and red surface for the back cell.) of a) ITO based tandem device, b) ultra-thin Ag based top-illuminated device without capping layer, c) ultra-thin Ag based top-illuminated device with 30 nm capping layer. Light intensity distribution in d) ITO based tandem solar cells, e) ultra-thin Ag based tandem solar cells without capping layer, f) ultra-thin Ag based tandem solar cells with 10 TeO2 as capping layer.

the single junction cells based on PIDTT-DFQT:$PC_{71}BM$ and PCPDT-FBT:$PC_{71}BM$ were shown in Figure 2. The detailed device parameters were summarized in Table 1. The PIDTT-DFQT:$PC_{71}BM$ micro-cavity device showed a V_{OC} of 0.91, a J_{SC} of 11.92 mA/cm^2, a FF of 0.60, and a PCE of 6.56%, which is slightly better than that of ITO based single junction device. Similarly, the PCPDT-DFBT:$PC_{71}BM$ micro-cavity device showed a better PCE (6.21%) than the ITO control device with a V_{OC} of 0.74 V, a J_{SC} of 15.07 mA/cm^2, and a FF of 0.56.

3.3 Optical Simulation of tandem device

Optical simulation was primarily performed to evaluate the optimum condition of the targeted tandem devices. In order to compensate the deviation between the calculated J_{SC} and measured J_{SC} arising from the assumption of 100% internal quantum efficiency (IQE), a mismatch factor of 0.95 and 0.61 is applied to the PIDTT-DFQT and PCPDT-FBT based BHJ devices, respectively. The origin of such mismatch factor is described in the experimental section. In Figures 4a-c, the green and red surfaces represent the BHJ thickness dependent J_{SC} of the front and back sub-cells, respectively. Balanced J_{SC} could be achieved along the cross line of the red and green surfaces. It is worthy to note that J_{SC} of the front sub-cell increased monotonously with the front cell's BHJ thickness while the back sub-cell showed the maximum J_{SC} at a BHJ thickness of 70-80 nm. Figure 4a depicted the BHJ thickness dependent J_{SC} of the sub-cells in the ITO-based tandem solar cell (device structure shown in Figure 1a).

As shown, the maximum J_{SC} could reach 8.8 mA/cm^2, where the BHJ thicknesses for the front and back sub-cells were 150 and 80 nm, respectively. However, for the PIDTT-DFQT:$PC_{71}BM$ single junction cell, the increase in BHJ thickness (or the charge transporting distance) would induce severe bimolecular charge recombination due to its low carrier mobility[25]. Thus, device performance would suffer a sharp drop in FF and PCE when the BHJ layer thickness is over 100 nm (Figure S1 and Table 1). Accordingly, the optimum device performance are expected to be obtained with front sub-cell thickness at 100 nm and back cell thickness at 80 nm, corresponding to a J_{SC} of 7.6 mA/cm^2 for the front cell and 9.3 mA/cm^2 for the back cell. For the series-connected tandem solar cells, the J_{SC} is controlled by the smaller one of the two sub-cells. Therefore, in the ITO based tandem solar cell, the maximum attainable J_{SC} is estimated as 7.6 mA/cm^2 limited by the front cell, and it creates the optical loss of 1.7 mA/cm^2 for the back cell.

For the ultra-thin Ag based top-illuminated tandem solar cells without capping layer (Figure 4b), the maximum balanced J_{SC} is 7.4 mA/cm^2, while the BHJ thicknesses are 180 nm and 60 nm for the front and back sub-cell, respectively. Considering the optimized BHJ layer thickness (<100 nm) of PIDTT-DFQT:$PC_{71}BM$ device, the highest attainable J_{SC} of this Ag based tandem solar cells without capping layer are expected to be only 5.1 mA/cm^2, where the thicknesses of the BHJ layers are 100 nm and 60 nm for the front and back sub-cell, respectively. The decrease in J_{SC} compared to the ITO-based counterpart could be attributed to the surface reflection optical loss and unbalanced J_{SC} between the two sub-cells. Fortunately, with the insertion of 30 nm TeO_2 as a capping layer, the maximum attainable front sub-cell J_{SC} is 7.3 mA/cm^2, while the J_{SC} of the back cell is 8.5 mA/cm^2. The increase in the maximum attainable J_{SC} of micro-cavity tandem device could be attributed to the suppressed reflection loss at Ag surface and the redistribution of the optical field intensity.

Apparently, similarly attainable JSC relative to the ITO-based configuration but with more balanced sub-cells' J_{SC} was obtained in the ultra-thin Ag based top-illuminated tandem device. Table S1 summarized the simulated J_{SC} of the front and back cell in tandem devices with different thickness of TeO_2 capping layer at fixed BHJ thicknesses in the front and back sub-cells of 100 nm and 80 nm, respectively. As shown, with the increase of TeO_2 layer, the J_{SC} of both sub-cells increased and reached the maximum at 30 nm for the front cells and 50 nm for the back cells. This verified that the deposition of TeO_2 layer could reduce the ultra-thin Ag surface reflection loss. The J_{SC} deviation of front and back cells also varied with the change of the capping layer thickness, suggesting the possibility of modulating the optical field distribution within the tandem device by tuning the capping layer thickness.

Figure 4 d-f showed the optical field distribution in the tandem solar cells. In the ITO-based tandem device, the light intensity was stronger due to the higher optical transmittance of ITO substrates and was delicately located in the BHJ region. However, due to unbalanced optical field distribution in the device, the J_{SC} of the front sub-cell cannot match that of the back sub-cell, resulting in the optical loss and imbalanced J_{SC}. In the top-illuminated tandem cell without TeO_2 capping, the optical field distribution in the tandem cell is weak due to the high reflectivity of the ultra-thin Ag layer. Moreover, the light intensity distribution is not equal in the front and back sub-cells. As a result, severe optical dissipation was created in this structure. However, through deposition of 30 nm TeO_2 capping layer on top of the ultra-thin Ag film, the reflection loss at the ultra-thin Ag surface was largely reduced and the optical field distribution in the two sub-cells became much balanced. With

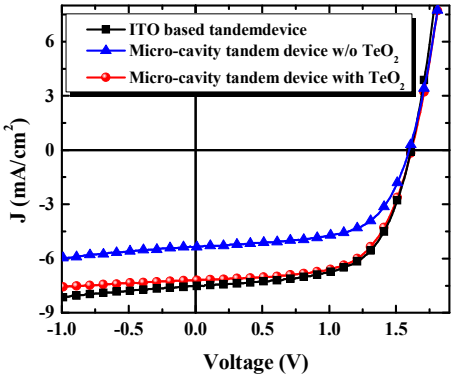

Figure 5. J-V characteristics of ITO based tandem solar cell, micro-cavity tandem solar cells without and with 30 nm TeO2 capping layer.

further increasing the thickness of the capping layer, the optical intensity inside the device also got enhanced, however, the center of the maximum optical intensity became gradually red-shifted (Figure S5). Finally, the compromise between the increased optical intensity and red-shifted maximum intensity determined that the best device performance should be achieved at 30 nm TeO_2. Figure S6 showed the simulated EQE spectra of the correspondingly constituent sub-cells. With the deposition of TeO_2, the light harvesting in both sub-cells got enhanced due to the reduced reflection loss at the Ag surface and were comparable to those of the ITO-based tandem solar cells. This result further affirmed that this ultra-thin Ag based micro-cavity configuration can enable the derived tandem device having the light-harvesting efficiency as sufficient as the ITO-counterpart despite the relatively lower transmittance of the ultra-thin Ag relative to ITO.

3.4 Top-illuminated tandem solar cells

Based on the optical simulation, three types of tandem devices were fabricated accordingly with the following structures: **Device C**: glass/ITO/ZnO/C_{60}-SAM/PIDTT-DFQT:$PC_{71}BM$/m-PEDOT:PSS/ZnO/C_{60}-SAM/PCPDT-FBT:$PC_{71}BM$/MoO_3/Ag; **Device D**: glass/Ag/MUA-SAM/ZnO/C_{60}-SAM/PCPDT-FBT:$PC_{71}BM$/m-PEDOT:PSS/ZnO/C_{60}-SAM/PIDTT-DFQT:$PC_{71}BM$/MoO_3/ultra-thin Ag (10 nm); **Device E**: glass/Ag/MUA-SAM/ZnO/C_{60}-SAM/PCPDT-FBT:$PC_{71}BM$/m-PEDOT:PSS/ZnO/C_{60}-SAM/PIDTT-DFQT:$PC_{71}BM$/MoO_3/ultra-thin Ag (10 nm)/TeO_2 (30 nm). If it is not specified, the thickness of the each layer is fixed as below: ITO: 120 nm, Ag: 100 nm, ZnO: 20 nm, PIDTT-DFQT:$PC_{71}BM$: 100 nm, m-PEDOT:PSS: 40 nm, PCPDT-FBT:$PC_{71}BM$: 80 nm, and MoO_3: 10 nm.

Figure 5 showed the J-V curves of Device C-E, and detailed device parameters were summarized in Table 2. It should be noted that all the V_{OC} of the tandem solar cells were nearly the summed value of the individual single junction cells, and the J-V curve showed normal diode rectification behavior. These confirmed the efficacy of the employed ICLs. The most distinct difference of the three devices was the J_{SC}, which is strongly dependent on the device architectures. For the ITO-based tandem devices, the high transparency of ITO substrate allows relatively large portion of solar irradiation to enter into the BHJ layers. Through controlling the thicknesses of constituent interlayers, the optical field can be more distributed in the BHJ layer region. As a result, Device C exhibited JSC up to 7.49 mA/cm^2, which is quite close to the optical simulation results (7.6 mA/cm^2). For Device D, a quite portion of light was reflected at the highly reflective ultra-thin Ag surface, and the optical loss causes a significant drop in J_{SC}. Consequently, J_{SC} of ~5.4 mA/cm^2 was obtained in this structure. However, after depositing a 30 nm TeO_2 capping layer, the J_{SC} of Device E significantly increased to 7.19 mA/cm^2 due to both the largely reduced reflection loss at ultra-thin Ag surface and the better balanced optical field distribution within the tandem device, consistent with the optical simulation (7.3 mA/cm^2). Finally, a comparable PCE of 7.4% to that (7.5%) of ITO-based tandem solar cells was accomplished in the top-illuminated ITO free tandem solar cell.

Table 2. Device parameters of tandem solar cells based on different transparent conductive electrodes (TCE)

TCE	TeO^2 [nm]	J_{SC} [mA/cm2]	V_{OC} [V]	FF [/]	PCE [%]
ITO	--	7.49	1.61	0.62	7.52(7.02±0.36)
Ultra-thin Ag	0	5.36	1.60	0.61	5.26(4.42±0.43)
	30	7.19	1.62	0.62	7.39(6.85±0.46)

[a]the PCE values outside of parentheses are the best device performance , and those inside indicate the averaged value and standard deviation.

4. Conclusions

In conclusion, an ultra-thin Ag based ITO-free tandem solar cell with micro-cavity configuration was demonstrated. Through depositing a 30 nm TeO2 capping layer on the ultra-thin Ag layer, the optical loss of the incident light at the reflective Ag surface was significantly reduced. Moreover, the optical field distribution in both sub-cells of the tandem device could also be modulated by this capping layer to result in a much balanced photocurrent between them. Finally, a PCE up to 7.4% comparable to that (7.5%) of ITO-based counterpart was demonstrated. Provided that the low cost and mechanical flexibility of ultra-thin Ag-based micro-cavity configuration, this study establishes a new feasible device architecture for the future development of efficient SCTOPV with highly printable compatibility.

Acknowledgements

A. K.-Y. Jen thanks the financial supports from the Air Force Office of Scientific Research (FA9550-09-1-0426), the Office of Naval Research (N00014-14-1-0170), the Asian Office of Aerospace R&D (FA2386-11-1-4072), and the Boeing-Johnson Foundation. This work was partly supported by the NSFC (No. 51473142) and the Major State Basic Research Program (973 program) (2014CB643503). L. Zuo thanks the China Scholarship Council (CSC) for the financial support.

References

1 A. J. Nozik, J. Miller, *Chem. Rev.* 2010, **110**, 6443; R. Gaudiana, C. Brabec, *Nat. Photon.* 2008, **2**, 287.
2 a) R. F. Service, *Science* 2011, **332**, 293; b) Y. Liu, C.-C. Chen, Z. Hong, J. Gao, Y. Yang, H. Zhou, L. Dou, G. Li, Y. Yang, *Sci. Rep.* 2013, **3**, 3356; c) Z. He, C. Zhong, S. Su, M. Xu, H. Wu, Y. Cao, *Nat. Photon.* 2012, **6**, 591; d) W. J. Potscavage, S. Yoo, B. Domercq, B. Kippelen, *Appl. Phys. Lett.* 2007, **90**, 253511; e) X. Hu, L. Chen, Y. Zhang, Q. Hu, J. Yang, and Y. Chen, *Chem. Mater*. 2014, **26**, 6293.
3 J. You, L. Dou, K. Yoshimura, T. Kato, K. Ohya, T. Moriarty, K. Emery, C.-C. Chen, J. Gao, G. Li, Y. Yang, *Nat. Commun.* 2013, **4**, 1446.

4 S. H. Park, A. Roy, S. Beaupre, S. Cho, N. Coates, J. S. Moon, D. Moses, M. Leclerc, K. Lee, A. J. Heeger, *Nat. Photon.* 2009, **3**, 297.
5 a) X. Guo, N. Zhou, S. J. Lou, J. Smith, D. B. Tice, J. W. Hennek, R. P. Ortiz, J. T. L. Navarrete, S. Li, J. Strzalka, L. X. Chen, R. P. H. Chang, A. Facchetti, T. J. Marks, *Nat. Photon.* 2013, **7**, 825; b) C. J. Brabec, S. Gowrisanker, J. J. M. Halls, D. Laird, S. Jia, S. P. Williams, *Adv. Mater.* 2010, **22**, 3839.
6 J. Y. Kim, K. Lee, N. E. Coates, D. Moses, T.-Q. Nguyen, M. Dante, A. J. Heeger, *Science* 2007, **317**, 222.
7 a) L. Zuo, C.-Y. Chang, C.-C. Chueh, S. Zhang, H. Li, A. K. Y. Jen, H. Chen, *Energy Environ. Sci.* 2015, **8**, 1712; b) J. You, C.-C. Chen, Z. Hong, K. Yoshimura, K. Ohya, R. Xu, S. Ye, J. Gao, G. Li, Y. Yang, *Adv. Mater.* **2013**, 25, 3973; c) T. Ameri, G. Dennler, C. Lungenschmied, C. J. Brabec, *Energy Environ. Sci.* 2009, **2**, 347; d) J. You, L. Dou, Z. Hong, G. Li, Y. Yang, *Prog. Poly. Sci.* 2013, **38**, 1909.
8 a) B. E. Lassiter, C. Kyle Renshaw, S. R. Forrest, *J. Appl. Phys.* 2013, **113**, 214505; b) A. Hadipour, B. de Boer, P. W. M. Blom, *Org. Electron.* 2008, **9**, 617.
9 a) L. Dou, J. You, J. Yang, C.-C. Chen, Y. He, S. Murase, T. Moriarty, K. Emery, G. Li, Y. Yang, *Nat. Photon.* 2012, **6**, 180; b) G. Dennler, M. C. Scharber, T. Ameri, P. Denk, K. Forberich, C. Waldauf, C. J. Brabec, *Adv. Mater.* 2008, **20**, 579; c) C.-H. Chou, W. L. Kwan, Z. Hong, L.-M. Chen, Y. Yang, *Adv. Mater.* 2011, **23**, 1282.
10 Y. Jin, J. Feng, M. Xu, X.-L. Zhang, L. Wang, Q.-D. Chen, H.-Y. Wang, H.-B. Sun, *Adv. Opt. Mater.* 2013, **1**, 809.
11 J. Yang, J. You, C.-C. Chen, W.-C. Hsu, H.-R. Tan, X. W. Zhang, Z. Hong, Y. Yang, *ACS Nano* 2011, **5**, 6210.
12 L. Zuo, C.-C. Chueh, Y.-X. Xu, K.-S. Chen, Y. Zang, C.-Z. Li, H. Chen, A. K. Y. Jen, *Adv. Mater.* 2014, **26**, 6778.
13 N. P. Sergeant, A. Hadipour, B. Niesen, D. Cheyns, P. Heremans, P. Peumans, B. P. Rand, *Adv. Mater.* 2012, **24**, 728.
14 K.-S. Chen, H.-L. Yip, J.-F. Salinas, Y.-X. Xu, C.-C. Chueh, A. K. Y. Jen, *Adv. Mater.* 2014, **26**, 3349.
15 H.-W. Lin, S.-W. Chiu, L.-Y. Lin, Z.-Y. Hung, Y.-H. Chen, F. Lin, K.-T. Wong, *Adv. Mater.* 2012, **24**, 2269.
16 X. Li, W. W. Cai, J. An, S. Kim, J. Nah, D. Yang, R. Piner, A. Velamakanni, I. Jung, E. Tutuc, S. K. Banerjee, L. Colombo, R. S. Ruoff, *Science* 2009, **324**, 1312.
17 a) H. Jin, C. Tao, M. Velusamy, M. Aljada, Y. Zhang, M. Hambsch, P. L. Burn, P. Meredith, *Adv. Mater.* 2012, **24**, 2572; b) J.-F. Salinas, H.-L. Yip, C.-C. Chueh, C.-Z. Li, J.-L. Maldonado, A. K. Y. Jen, *Adv. Mater.* 2012, **24**, 6362.
18 D. Gupta, M. M. Wienk, R. A. J. Janssen, *ACS Appl. Mater. Interf.* 2014, **6**, 13937.
19 C.-Y. Chang, L. Zuo, H.-L. Yip, Y. Li, C.-Z. Li, C.-S. Hsu, Y.-J. Cheng, H. Chen, A. K. Y. Jen, *Adv. Funct. Mater.*2013, **23**, 5084.
20 Y. Zhang, J. Zou, C.-C. Cheuh, H.-L. Yip, A. K. Y. Jen, *Macromolecules* 2012, **45**, 5427.
21 Y.-X. Xu, C.-C. Chueh, H.-L. Yip, F.-Z. Ding, Y.-X. Li, C.-Z. Li, X. Li, W.-C. Chen, A. K. Y. Jen, *Adv. Mater.* 2012, **24**, 6356.
22 a) S. K. Hau, H.-L. Yip, K.-S. Chen, J. Zou, A. K.-Y. Jen, *Appl. Phys. Lett.* 2010, **97**, 253307; b) C.-C. Chueh, C.-Z. Li, A. K. Y. Jen, *Energy Environ. Sci.* 2015, **8**, 1160.
23 M. Lenes, L. J. A. Koster, V. D. Mihailetchi, P. W. M. Blom, *Appl. Phys. Lett.* 2006, **88**, 243502.
24 G. F. Burkhard, E. T. Hoke, M. D. McGehee, *Adv. Mater.* 2010, **22**, 3293.
25 A. Guerrero, N. F. Montcada, J. Ajuria, I. Etxebarria, R. Pacios, G. Garcia-Belmonte, E. Palomares, *J. Mater. Chem. A* 2013, **1**, 12345.

Manipulation of Optical Field Distribution in ITO-free Micro-cavity Polymer Tandem Solar Cell via the Out-of-cell Capping layer for High Photovoltaic Performance

Lijian Zuo,[ab]† Chih-Yu Chang,[a]† Chu-Chen Chueh,[a] Yunxiang Xu,[a] Hongzheng Chen[b] and Alex K.-Y. Jen*[ab]*

[a]Department of Materials Science and Engineering, University of Washington, Seattle, USA. E-mail: ajen@u.washington.edu

[b]State Key Laboratory of Silicon Materials, MOE Key Laboratory of Macromolecular Synthesis and Functionalization, Department of Polymer Science & Engineering. Email ajen@u.washington.edu, hzchen@zju.edu.cn

† These authors contributed equally.

Keywords: ITO-free, micro-cavity, tandem solar cells, ultra-thin Ag

The out-of-cell capping layer of an ITO-free microcavity series-connected tandem organic photovoltaic device (SCTOPV) plays an important role on manipulating the optical field distribution in the constituent sub-cells for achieving balanced photocurrents and the optimal photovoltaic performance. Two mirror-like electrodes, including a semi-transparent ultrathin Ag capped with a dielectric TeO_2 layer, are used to construct an indium tin oxide (ITO)-free top-illuminated microcavity configuration, in which certain frequencies of solar irradiance can resonate between the reflective surfaces. It is unveiled that the distribution of light intensity within the sub-cells can be easily manipulated by controlling the thickness of TeO_2 capping layer. As a result, a top-illuminated ITO-free, SCTOPV, with the comparable performance (7.4%) to ITO-based counterpart is demonstrated despite the inferior transmittance of ultrathin Ag compared to ITO.